ACS NANO

www.acsnano.org

ARTICLE

Stretchable, Self-Healing, and Skin-Mounted Active Sensor for Multipoint Muscle Function Assessment

Chan Wang,[#] Xuecheng Qu,[#] Qiang Zheng,[#] Ying Liu, Puchuan Tan, Bojing Shi, Han Ouyang, Shengyu Chao, Yang Zou, Chaochao Zhao, Zhuo Liu, Yusheng Li,* and Zhou Li*

Cite This: https://doi.org/10.1021/acsnano.1c02010 Read Online

ABSTRACT: Assessment of muscle function is an essential indicator for estimating elderly health, evaluating motor function, and instructing rehabilitation training, which also sets urgent requirements for mechanical sensors with superior quantification, accuracy, and reliability. To overcome the rigidity and vulnerability of traditional metallic electrodes, we synthesize an ionic hydrogel with large deformation tolerance and fast self-healing ability. And we propose a stretchable, self-healing, and skin-mounted (Triple S) active sensor (TSAS) based on the principles of electrostatic induction and electrostatic coupling. The skin modulus-matched TSAS provides outstanding sensing properties: maximum output voltage of 78.44 V, minimal detection limit of 0.2 mN, fast response time of 1.03 ms, high signal-to-noise ratio and excellent long-term service stability. In training of arm muscle, the functional signals of biceps and triceps brachii muscles as well as the joint dexterity of bending angle can be acquired simultaneously through TSAS. The signal can also be sent wirelessly to a terminal for analysis. With the characteristics of high sensitivity, reliability, convenience, and low-cost, TSAS shows its potential to be the next-generation procedure for real-time assessment of muscle function and rehabilitation training.

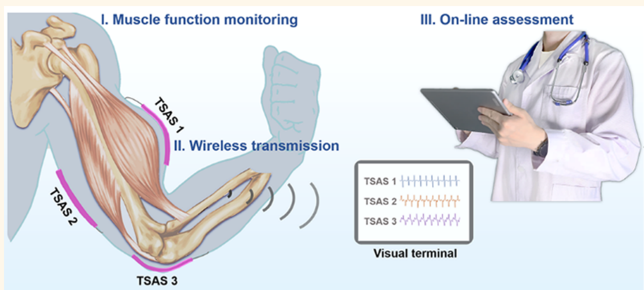

KEYWORDS: *self-healing hydrogel, muscle function assessment, skin-mounted, self-powered, triboelectric nanogenerator*

In 2015, WHO proposed a report entitled "World Report on Aging and Health", which clarified that the goal of healthy aging is to help people in developing and maintaining the functional ability that enables well-being. It is well-known that muscle function is one of the most critical functional abilities of the human body. It declines with age and can be impaired under a variety of medical conditions.[1,2] Assessing muscle function in daily clinical practice would be helpful for clinicians of the elderly and frail.[1,3,4] Although a large number of approaches to assess muscle function have been proposed, such as Manual Muscle Testing (MMT), Field Testing, Hand-Held Dynamometry (HHD), and Hand-Grip Dynamometry (HGD), clinicians still need to select a more reliable, validated, and appropriate method for the patients, since these approaches have their intrinsic limitations.[5−8]

MMT and Field Testing are influenced by subjective tester judgment and lack of normative values.[7] HHD provides accurate detection but is influenced by tester strength, and its expensive equipment limits its use in clinical practice. HGD has outstanding clinical properties, while it is only adapted to the measurement of grip strength.[8] In addition, all these methods typically assess the overall function of actions (*e.g.*, Curl) rather than individual muscles or muscle groups (*e.g.*, Biceps), which is actually more important for precise diagnosis. Their absolute values and precision may also be influenced by various factors, such as positions, postures, body weight, external resistance, and environment.[6,7] Therefore, more advanced tools with objectivity, accuracy, reliability, convenience, and low cost should be developed by quantitative methods for diagnosis and timely intervention of individuals with muscle dysfunction in order to prevent and delay the progression of the disease.

Triboelectric nanogenerator (TENG),[9−14] which is based on the principles of electrostatic induction and charge coupling

Received: March 8, 2021
Accepted: June 3, 2021

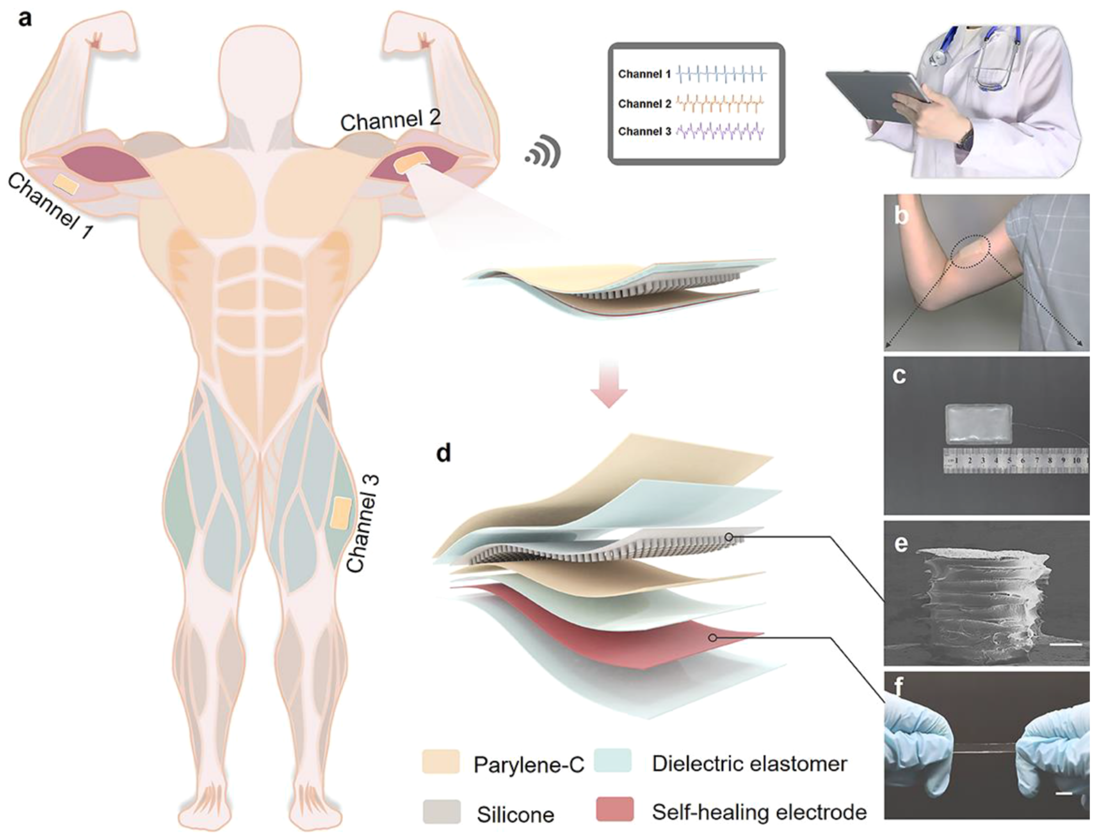

Figure 1. Schematic illustration of TSAS for assessment of muscle function. (a) The TSAS can be attached to the body's muscles for real-time muscle function monitoring. (b) The TSAS could be well attached to the biceps brachii. (c) The TSAS was designed with a size of 3 cm × 5 cm. (d) Materials and overall assembly of the TSAS. The dielectric elastomer deposited with 3 μm parylene-C was used as top packaging and bottom friction layer. The silicone with surface microstructure was used as the top friction layer. The self-healing ionic hydrogel was used as an electrode. (e) SEM image of the microcolumn on the silicone film. Scale bar: 300 μm. (f) Optical image of the self-healing ionic hydrogel shows superior transparency and stretchability. Scale bar: 1 cm.

has shown significant advantages in active sensing of various physical signals,[15,16] like biomechanical forces,[17] strain,[18] pressure,[19] and body motions.[20] Owing to its features of high sensitivity, reliability, light weight, and low cost,[21−23] TENG seems to be an ideal candidate for muscle function monitoring. Unfortunately, the mechanical mismatch of TENG with tissues will significantly affect its accuracy of signal measurement, and the fragility of its metallic electrode layer under repeated deformation also constrains its further application in biological systems.[24,25]

In this paper, we report a stretchable, self-healing, and skin-mounted active sensor (TSAS) based on TENG, which can measure the function of multiple muscle groups involved in the training of arm muscle. Firstly, we prepared a magical ionic hydrogel with fast self-healing property, stretchability, and conductivity to replace the traditional metal electrode layer of TENG, providing TSAS with excellent flexibility, durability, and skin adhesion ability. Subsequently, we established the relationship between the output signal of TSAS and the applied force for further functional analysis of muscle strength by a systematic *in vitro* experiment. Finally, the TSASs were attached to multiple muscle groups involved in the training of arm muscle, and the functional signals from biceps brachii and triceps brachii were then acquired. Through equipping with a Bluetooth transmitter, real-time data from TSAS were transmitted to the terminal unit. Compared with traditional tools for the assessment of muscle function, the TSAS can objectively quantify muscle strength, which is vertical to the direction of contraction, and measure joint bending angle, while also providing high sensitivity, reliability, convenience, low-cost, and self-powered ability, showing an expectation in the assessment of muscle function and training of rehabilitation.

RESULTS AND DISCUSSION

Selection of the Materials and Design of the Device. To achieve accurate, reliable, and convenient assessment of muscle function, conformal and real-time measurement of single muscle and muscle groups is necessary. We proposed a stretchable, self-healing, and skin-mounted TENG-based active sensor (TSAS) to meet these requirements. With a wireless transmitter, real-time assessment of muscle function and guidance of rehabilitation training is achievable (Figure 1a). Taking full account of the tissue modulus (about 0.1−100 kPa)[26] and large deformation (max up to 66%)[27] during sports training, the TSAS was built to be fully stretchable and flexible (Figure 1b,c). TSAS consists of seven layers, in which ionic hydrogel (Figure 1f) was synthesized as an electrode, silicone rubber and parylene-C (middle) were selected as friction layers, and dielectric elastomer (VHB) and parylene-C (top) serviced as the substrate and packaging layers (Figure 1d). The surface of a silicone film was structured with microcolumns to keep a distance from two friction layers and play a supporting role (Figure 1e and Figure S1). The VHB helped the device to

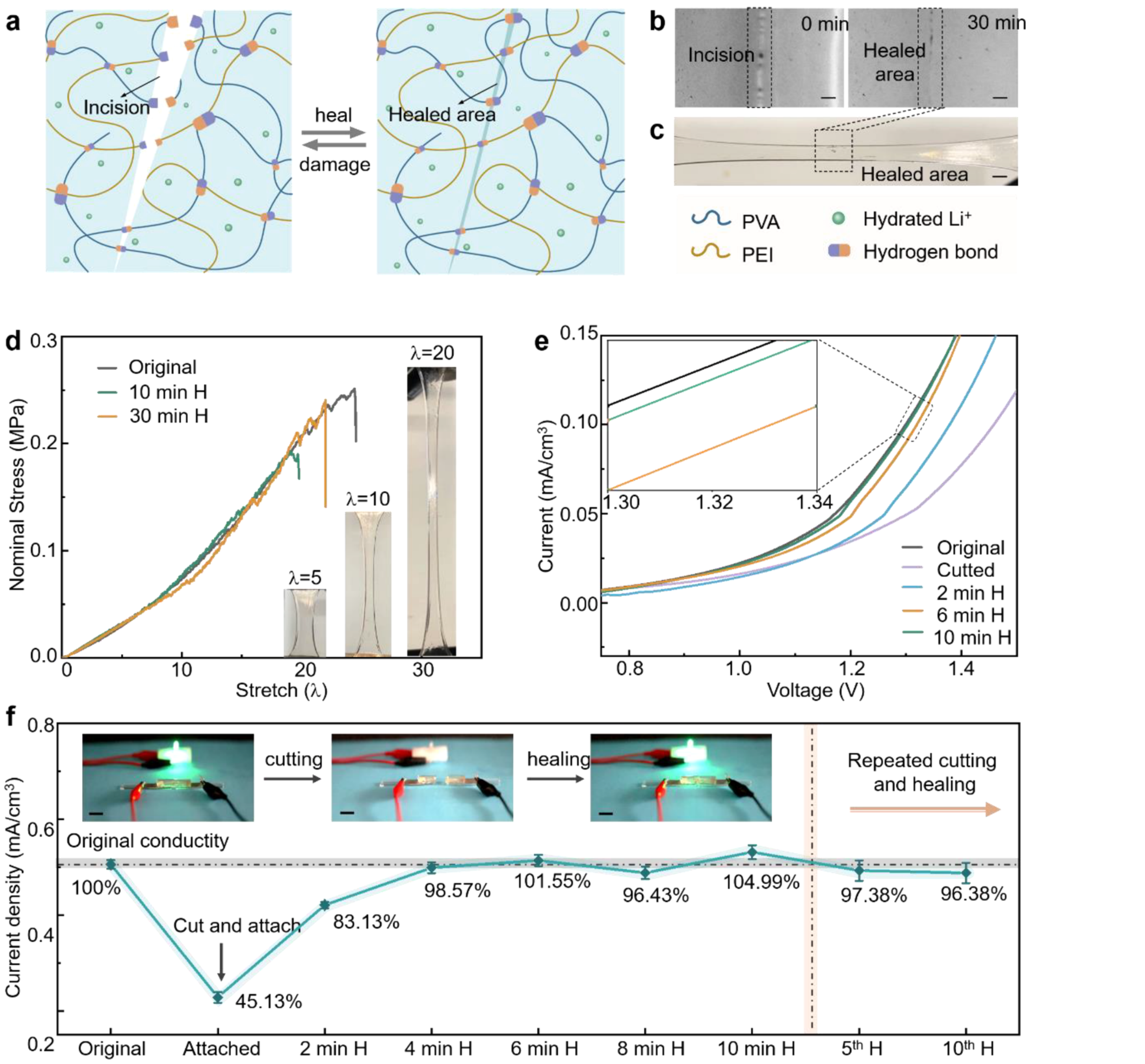

Figure 2. Design principle and properties of the self-healing electrode. (a) Self-healing mechanism of the electrode. (b) Photographs about the self-healing process of the electrode. After 30 min, the incision disappeared. Scale bar: 20 μm. (c) The healed area could afford big deformation without rupture. Scale bar: 0.5 cm. (d) Tensile strain−stress curves of the electrode. The inset displayed the healed sample in the state of 5, 10, and 20 times tensile deformation. Original sample size: 20 × 10 × 2 mm^3. Tensile speed: 50 mm·min^{-1}. (e) and (f) Conductivity of the electrode at different self-healing time and self-healing cycles. The insets of (f) were the electrode connected in the circuit to lighten a LED.

avoid outside interference and secure the sensor on the skin tightly. It should be pointed out that the packaging of the electrode protects ionic hydrogel from exsiccation and maintains a dry environment between two friction layers, which is essential for the output of TENG. With the customized structure, TSAS possessed abilities to mount on the skin tightly, react sensitively to muscle state change, and to have multipoint simultaneous measurements, which is the basis for achieving real-time muscle function assessment and professional data analysis via wireless transmission.[28,29]

As a key component, the electrode, which was based on an ionic hydrogel, was designed to be flexible, stretchable, conductive, and self-healing for TSAS.[12,30−34] Compared with the traditional metallic electrode, the ionic hydrogel performed superiority on a good modulus, which can match with tissues.[26,35] The ionic hydrogel was fabricated with proportioned poly(vinyl alcohol) (PVA), polyethylenimine (PEI), and lithium chloride (LiCl), forming a nanostructure based on polymer segments entanglement and dynamic hydrogen bonds.[36] The long molecular chain of PVA and the short molecular chain of PEI constitute the supporting skeleton. Meanwhile, the hydrated Cl^- and Li^+ filled the lacuna of the system and help to form dynamic hydrogen bonds.[37] When the hydrogel was stretched, the system dissipated energy by breaking and re-forming dynamic bonds as well as the relative slipping between molecular chains.[38] Once the ionic hydrogel was damaged, the reconstruction of dynamic hydrogen bonds and polymer segments helps to restore the injured area to its original appearance and function.[39] The corresponding conceptual diagram of the hydrogel and the healing process were exhibited in Figure 2a. To deeply understand the autonomous self-healing performance, extreme mechanical damage was created by separating the hydrogel completely into two parts, and then the healing process was observed after the damaged hydrogel was brought together slightly. On the basis of the reconstruction of dynamic

https://doi.org/10.1021/acsnano.1c02010
ACS Nano XXXX, XXX, XXX−XXX

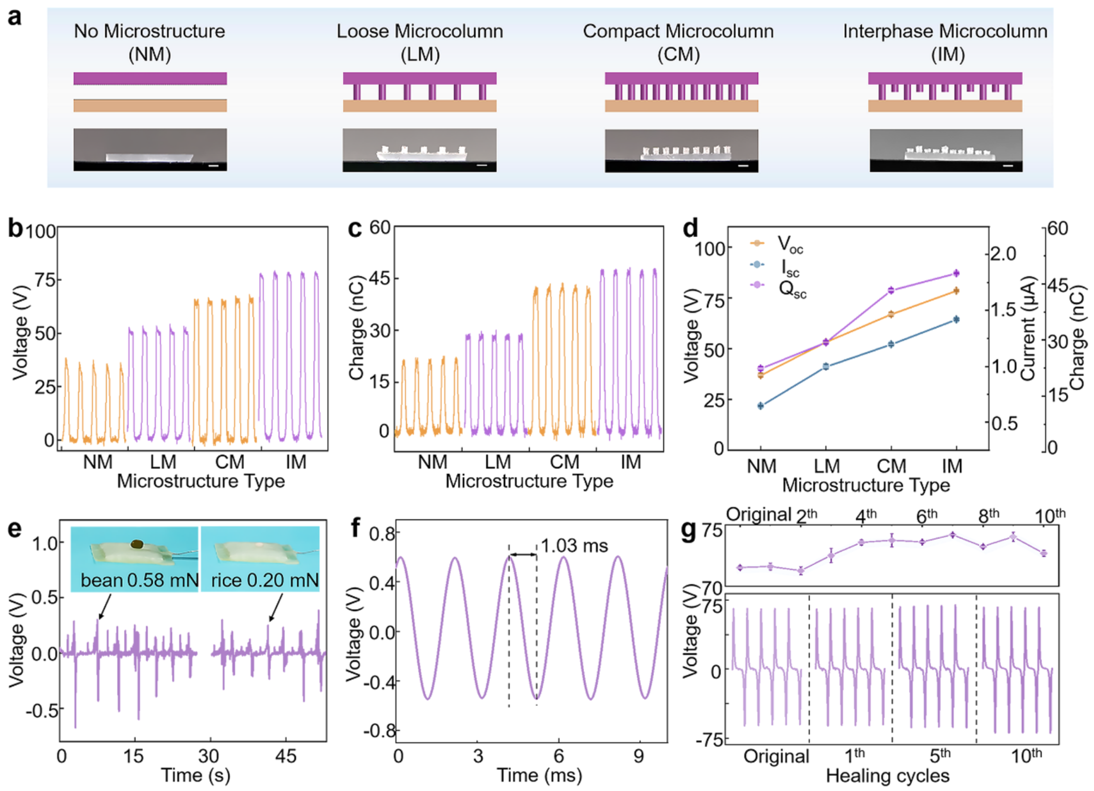

Figure 3. Electrical characteristics of TSAS. (a) Four types of microstructure on friction layer were designed, including none microstructure (NM), loose microcolumn (IM), compact microcolumn (CM), and interphase microcolumn (IM). Scale bar: 1 mm. V_{oc} (b) and Q_{sc} (c) curves of the TSAS with four types of friction layer. (d) The V_{oc}, I_{sc}, and Q_{sc} value of TSAS with four types of friction layer. (e) TSAS can distinguish the rice (0.2033 mN) and mung bean (0.5843 mN). (f) V_{oc} of TSAS tested with a high frequency of 500 Hz. (g) V_{oc} of TSAS after different self-healing cycles.

interactions and polymer segments, the morphology and function of the hydrogel recovered quickly. After 10 min of healing, the incision grew together (Movie S1 and Figure S2) and entirely disappeared within 30 min at room temperature (Figure 2b,c). The mechanical healing efficiency of the hydrogel was explored through tensile experiments (Figure 2d). The nominal stress−strain curves of pristine hydrogel performed as an elastomer with excellent mechanical properties,[40] showing about 2440% fracture deformation and 0.25 MPa breaking strength. After cutting and 10 min of healing, the breaking strain could recover to 80.48% of max fracture deformation. For a longer healing time of 30 min, the recovery effect could reach about 93.94%. The insets showed the samples at 5, 10, and 20 times the stretching ratio.

Besides, the self-healing behavior of the electrode materials was also systematically explored. The current−voltage curves of the hydrogel (Figure 2e), which was mainly attributed to ions participating in conduction performed similarly to semiconductors. Along with the increase of voltage, more conductive paths formed. Hence the conductivity rose.[39] The electrical performance recovered to the pristine state in less than 6 min after cutting and attaching the hydrogel. Furthermore, we performed a greater number of cutting/healing cycles (Figure 2f). After the 10th healing, the conductivity of the hydrogel remained above 95%. The inset images showed the hydrogel as a conductor to connect a LED with a power supply, when the damaged parts were attached together, the LED lit at once. The as-fabricated ionic hydrogel with outstanding stretchability and superior healing ability gave the active sensor sufficient durability to withstand repeated deformations and accidental damage, which satisfy the requirements of the electrode material in the TSAS.

Structural Optimization, Electrical, and Self-Healing Properties Characterization of TSAS. The detecting ability of TSAS is closely related to its electrical output. A large electrical output enables a highly sensitive sensor.[41] With the change contact area, the surface structure of the friction layer is important for the output performance of TSAS. TSAS with four types of friction layers were designed, including none microstructure (NM), loose microcolumn (LM), compact microcolumn (CM), and interphase microcolumn (IM) (Figure 3a, Figure S3 and Figure S4). A linear motor with the same vertically compressive force was employed to measure the electrical output performance of TSAS with these four friction layers. As shown in Figure 3b,c and Figure S5, the open-circuit voltage (V_{oc}), short-circuit current (I_{sc}), and short-circuit transferred charge (Q_{sc}) were related to microcolumn density and the arrangement pattern. The TSAS with the IM fraction layer presented the highest electrical output with V_{oc}, I_{sc}, and Q_{sc} reaching 78.44 V, 1.42 μA, and 47.48 nC, respectively (Figure 3d). These differences may be accredited to the actual contact area of friction layers being further increased owing to the deformable microstructures and more charge transfer paths generated by the compact microcolumns.

The minimum detection limit of the optimized TSAS, as well as its minimum response time and tensile fatigue resistance, were systematically explored.[42] The TSAS could effectively detect a force as light as 0.2 mN, which was equivalent to the weight of a grain of rice (Figure 3e and

https://doi.org/10.1021/acsnano.1c02010
ACS Nano XXXX, XXX, XXX−XXX

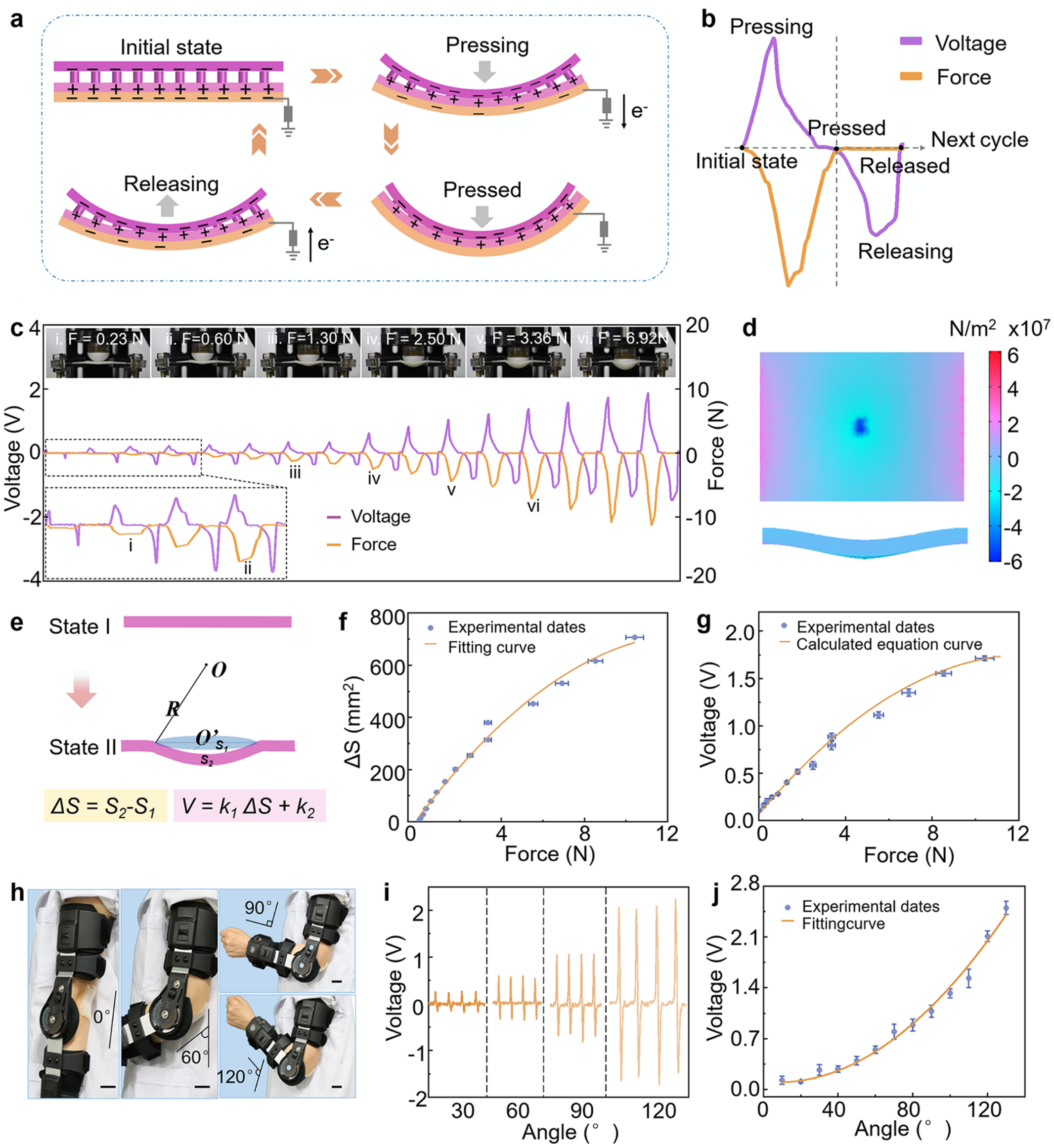

Figure 4. Research about the relationship between the output voltage of TSAS and the applied force. (a) Schematic illustration about the working principle of TSAS. (b) Curves of V_{oc} and corresponding applied force during one working cycle. (c) V_{oc} curves of TSAS under different pressing force. The curve pulses marked as i−vi were in accordance with optical images displayed at the top of (c). (d) Simulation of the force distributing on the sensor when TSAS was pressed by a total force of 0.102 N. (e) Schematic illustration about contacted area change (ΔS) of TSAS during force applying. The V_{oc} and ΔS satisfy a linear relationship of $V_{oc} = k_1\Delta S + k_2$. (f) The ΔS and pressing force satisfy the equation $\Delta S(F) = 14.14 + 105.4F - 3.96F^2$. The experimental data and fitting curve were represented by scatters and solid line, respectively. (g) The relationship of the output voltage of TSAS and force satisfy eq 2: $V_{oc}(F) = 0.085 + 0.247F - 0.00919F^2$. The experimental data and calculated equation show good matching curves. The scatters and solid line respect experimental data and calculated equation. (h) Pictures of the TSAS adhered on the elbow. (i) Voltage curves of TSAS when the elbow was at 30°, 60°, 90°, 120°. Scar bar: 2 cm. (j) The V_{oc} of the TSAS at different bending angles satisfy eq 3: $V_{oc}(\theta) = 0.08 - 0.0011\theta + 1.425 \times 10^{-4}\theta^2$. The experimental data and fitting curve were represented by scatters and the solid line, respectively.

Movie S2). Besides, the TSAS could distinguish the mechanical vibration at a frequency of 500 Hz generated by the vibration platform, demonstrating an excellent time response (Figure 3f). After a 10^5 times cycle test using a linear motor at a frequency of 2.5 Hz, the TSAS retained outstanding stability (Figure S6). Then the self-healing performance of TSAS was studied by creating extreme physical damage: cutting the sensor into two parts and then attaching the two parts slightly. After 1 min of healing, the V_{oc} of healed TSAS was tested and its output almost undecayed. As for more breaking and healing times, the output performance of the device was well retained, which indicated excellent self-healing ability and durability of the device (Figure 3g and Movie S3)

Research about the Relationship between the Output Voltage of TSAS and the Applied Force. To take the advantages of the structural design and further apply it to muscle function measurement, it is necessary to explore the relationship between the output behavior of TSAS and the external function applied on the device. The working mechanism of TSAS at the open-circuit state is summarized in Figure 4a and Figure S7.[43,44] On the principle of the coupling of contact electrification and electrostatic induction, once the sensor was subjected to an external force, the surfaces

https://doi.org/10.1021/acsnano.1c02010
ACS Nano XXXX, XXX, XXX−XXX

of both friction layers would carry different charges while the electrode was equipped with equal amounts of negative charges. The charge density remained stable due to the open-circuit and dielectric properties of silicone and parylene-C, while the induced charge on the electrode would vary along with the contact area and distance of two friction layers.[44] The conduction mechanism for electricity transport is attributed to Maxwell's displacement current,[45] which can be defined as:

$$J_D = \frac{\partial D}{\partial t} = \varepsilon_0 \frac{\partial E}{\partial t} + \frac{\partial P}{\partial t}$$

where J_D is the free electric current density, D is displacement field, ε_0 is permittivity in vacuum, E is the electric field, and P is the polarization field. In one working cycle, the states of TSAS are defined as stretching and restoring parts. During the stretching process, trigged by mechanical force, the friction layers of TSAS were pressed face to face, with the increasing contact area, partly positive charge synchronous flowed out of the electrode at the force of the electric field. When the external force reaches the maximum, two friction layers were fully touched and generated the largest contacted area under the big deformation, while the induced charge on the electrode was completely transferred out. In the following restoring process, with force evacuating, the friction layers recovered the deformation under its intrinsic elasticity and then separated, the charge flowed back to the electrode until the initial state.[31,46−48] The corresponding force and electrical signals are shown in Figure 4b, which are in a periodic and matchup relationship.

Next, the specific relationship between V_{oc} of TSAS and the applied force was explored. We acquired the multigroup electrical and force signal by an oscilloscope and Mark-10 test system. A polymer hemisphere with a diameter of 3 cm was attached to the force detector to mimic muscle-induced deformation of the TSAS during the test (Figure 4c and Movie S7). The V_{oc} of TSAS rose sensitively with the little force and increased when the force was larger than 7 N. The simulation of force distribution in Figure 4c-ii illustrated that the force was uneven throughout the sensor, where the middle position was subjected to the greatest force (Figure 4d).

According to the capacitance model and Maxwell's displacement current, the V_{oc} is related to the change of contacted area and separated distance between friction layers.[21] The separated distance in this work is an approximate constant, so the V_{oc} is mainly affected by contacted area change (ΔS, the calculated method shown in Figure S8 and Note S1). We assumed that the V and ΔS satisfy eq 1, as displayed in Figure 4e.

$$V_{oc} = k_1 \Delta S + k_2 \quad (1)$$

where k_1 and k_2 are undetermined coefficients and k_2 is introduced as a constant that includes other factors, such as the roughness of friction layers and edge effect.[44] It is important that the deformation (the same as ΔS) is linearly related to the force with a consistent specification parameter of TSAS (Figure 4f). Thus, eq 2 about V_{oc} and force was obtained and written according to the bridge-like parameter (ΔS) and experimental data:

$$V_{oc}(F) = 0.08506 + 0.2466F - 0.009196F^2 \quad (2)$$

V and F satisfy the binomial relationship. The equation curve shows good coincidence with experimental data (Figure 4g). More details about calculated methods and processes can be found in Figures S9−S11; Notes S1−S3 and Table 1. Besides,

Table 1. Experimental Data Used in This Work[a]

H (mm)	force (N)	ΔS (mm^2)	voltage (V)
1	0.03516	3.14	0.10698
3	0.22892	28.26	0.1605
4	0.37125	50.24	0.2062
5	0.60448	78.5	0.24644
6	0.88062	113.04	0.28136
7	1.29022	153.86	0.4036
8	1.7898	200.96	0.5159
9	2.49722	254.34	0.58327
10	3.3554	314	0.79362
11	3.35459	379.94	0.88605
12	5.5262	452.16	1.11468
13	6.9164	530.66	1.35061
14	8.53061	615.44	1.55433
15	10.41982	706.5	1.71271

[a]The force and voltage data are mean values from multiple trials.

the effect of the hemisphere's speed on the output of TSAS was also taken into account. The speed showed a much smaller effect on the output of TSAS compared to force (Figure S12). Even though, to ensure the accuracy of the results, the test speed used in this work was fixed at 1 m·s^{-1}.

As we know, muscle strength and the flexibility of relative joints are equally important in a complete assessment of muscle function. Therefore, TSAS was also used to detect the bending angle of the elbow, which was related to the flexibility of the joint. By fixing the bendable elbow angle with controller (Figure 4h), we measured the V_{oc} of TSAS at a specific angle (Figure 4i) and obtained the relationship of the output voltage and the bending angles (θ) through a linear fitting, which satisfy the eq 3 (Figure 4j):

$$V_{oc}(\theta) = 0.08 - 0.0011\theta + 1.425 \times 10^{-4}\theta^2 \quad (3)$$

TSAS Used for Muscle Function Monitoring. On the basis of the superior performance of electrical output and splendid sensing property to force, TSAS can be used to monitor muscle function. During the activity of the human body, the extensor and flexor always appear in pairs to complete a set of movements,[3,8] such as the biceps brachii (BB) and triceps brachii (TB) are a group of corresponding muscles. When the arm lifted, the BB contracted to move the bone while the TB relaxed, which was contrary to the straightening arm. Taking advantage of the flexible and stretchable, TSAS can be accurately attached to the skin of the BB, TB, and elbow.

With contraction/relaxation of the targeted muscles and bending of the elbow, TSAS would then be compressed and released, converting mechanical signals into voltage signals simultaneously (Figure 5a). In this work, volunteers' muscle strength vertical to the direction of contraction (MSV) was tested by lifting and straightening arms without load and loading weight on 3 kg dumbbell, respectively (Figure 5b). The V_{oc} signals of TSAS were collected synchronized by the oscilloscope (Figure 5c). The results showed that the signal amplitude of the BB and TB with loading was larger than that without load, owing to more power being needed to overcome the gravity of the dumbbell, while the signal of elbow showed an opposite tendency because it is toilsome to lift a dumbbell. The state of the muscles could be estimated from the signal waveform. The positive (negative) peak corresponding to the contracting (relaxing) of muscle and the bending (recovering)

https://doi.org/10.1021/acsnano.1c02010
ACS Nano XXXX, XXX, XXX−XXX

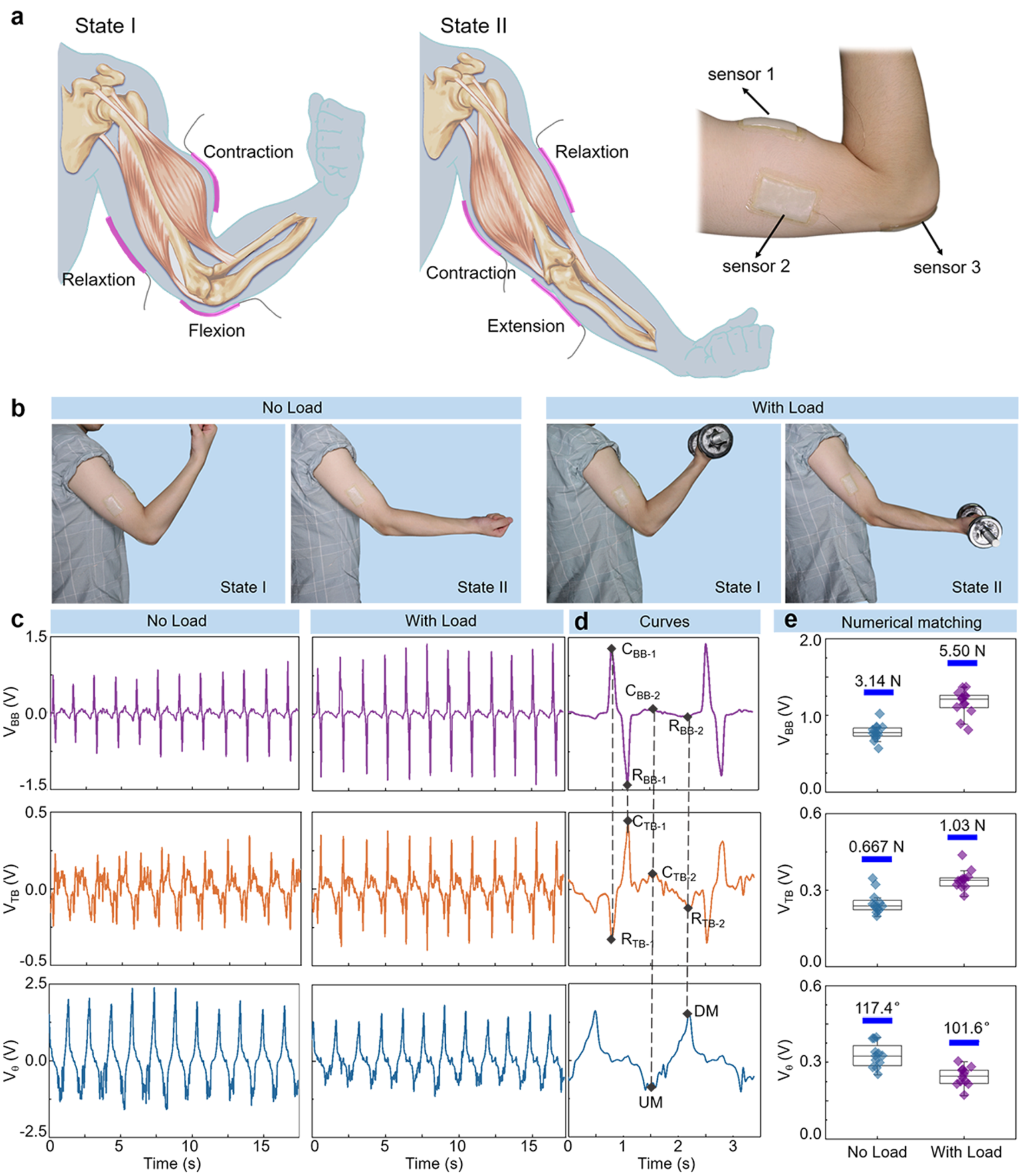

Figure 5. TSAS used for muscle function assessment. (a) Schematic illustration of the TSAS's working process in a set of arm movements. The right inset was a picture of TSAS monitoring muscle strength. (b) Pictures about TSAS used in muscle function monitoring through arm bending motion without/with a load. (c) V_{oc} of TSAS adhered on biceps brachii (V_{BB}), triceps brachii (V_{TB}), and elbow (V_θ), respectively. Two states of without/with load were explored. Details about voltage curves of V_{BB}, V_{TB}, and V_θ were shown in (d). (e) The value of muscle strength, elbow' 's bending angle could be calculated through eqs 2 and 3.

of the elbow. In detail, the curve characteristics also demonstrated information about muscle function, as shown in Figure 5d. From state I to state II, the arm moved from the highest point to the lowest point, the BB transformed from contraction (C_{BB-1}) to relation (R_{BB-1}), and the TB changed from a relaxed state (R_{TB-1}) to a contracted state (C_{TB-1}). It should be noted that the TB has two muscle fiber bundles, so there were two contraction peaks (C_{TB-1}, C_{TB-2}) after the relaxation peak (R_{TB-1}). Due to the impact of the TB, the BB induced a set of small peaks (C_{BB-2}, R_{BB-2}). The signal peaks (UM, DM) from the bending elbow were opposite to the peaks (C_{TB-2}, R_{TB-2}) of the TB in the movement. In addition, the same tests were carried out on other volunteers. The results were collected and summarized in Figures S13 and S14 and Movies S5 and S6. A similar phenomenon about V_{oc} of TSAS could be found; however, there was some difference of peak amplitude due to individual difference. Furthermore, the MSV could be obtained through the value of forwarding peak amplitude, eq 2, and eq 3. The MSV of a volunteer's BB and TB were 3.14 N, 0.667 N on the state of unloaded, as well as the bending angle of the elbow was 117.4°. When there was a load of 3 kg dumbbell, the myodynamia of the BB and TB and

https://doi.org/10.1021/acsnano.1c02010
ACS Nano XXXX, XXX, XXX−XXX

the bending angle of the elbow were 5.50 N, 1.03 N, and 101.6°, respectively (Figure 5e). Moreover, other muscles like gastrocnemius, tibialis anterior, and vastus lateralis could also be tested in this system (Figure S15). The monitoring of muscle strength and elbow bendable angles is of great importance in the assessment of muscle function. Through analysis of these data, the health and state of muscles can be learned, which could provide quantifiable, objective, accurate, and reliable support in clinic treatment. Finally, with the help of a Bluetooth transmitter, the acquired data from TSAS could be transmitted to the intelligent terminal (Movie S7 and Figure S16 and S17), which is expected to be applied in on-line elderly health assessment, motor function evaluation, and rehabilitation training guidance.

CONCLUSION

In this work, we proposed a stretchable, self-healing, and skin-mounted active sensor for multipoint muscle function monitoring. Firstly, an innovative self-healing ionic hydrogel was synthesized to overcome the vulnerability of traditional metallic electrode in TENG during long-term service with large deformation. Then, a self-powered and muscle modulus-matched sensor was designed and fabricated based on the self-healing electrode accompany with stretchable silicone and parylene-C, which possesses a maximum output of 78.44 V, a low detection limit (0.2 mN), a fast response time (1.03 ms), and a long service life (continuous 10^5 tests without performance degenerating). The output of TSAS remained stable, even after 10 times damaging and healing processes. Next, a mechanical model was developed to explore and determine the relationship between TSAS electrical signals and applied stress, which can be further used to assess muscle strength. In actions of arm muscle training, the kinestate and MSV of the BB and TB were detected and recorded as the electrical signal and the bending angles of the elbow. Through a wireless transmission module, the as-produced data could provide valid online information for the assessment of elderly health, evaluation of motor function, and guidance of rehabilitation training.

Compared to traditional muscle measurement equipment, TSAS can provide more accurate personal service with the advantages of (i) direct and quantitive monitoring of muscle strength and joint curvature; (ii) interference-free testing with mounting on the skin of muscle; (iii) good selectivity of distinguishing single-muscle strength from group muscles; (iv) multipoint simultaneous measurement; (v) small size, light weight, and easy operation; (vi) no required external power supply. It is credible that with the development of the technology of TSAS, the assessment of muscle function will be more convenient. However, there is still space for improvement in terms of structural optimization, performance improvement, and application scenario expansion. Further research will focus on the development of an intelligent feedback muscle rehabilitation training system, including synchronous multipoint signal acquisition and real-time analysis of measured signals for patients.

EXPERIMENTAL SECTION

Materials. Poly(vinyl alcohol) (PVA, CAS: 9002-89-5, 1799, P105126) and polyethylenimine (PEI, CAS: 9002-98-6, M_W = 600, E808878) were purchased from Aladdin. Lithium chloride (LiCl, CAS: 7447-41-8, L812571) was purchased from Macklin. Silicone rubber (Ecoflex 00-30) produced by Smooth-On, Inc. Parylene-C (poly(chloro-*p*-xylene)) with CAS 28804-46-8 was produced by Specialty Coating Systems, Inc. VHB (3MF9460PC) mainly based on acroleic acid was purchased from Shenzhen LaiRunPu Technology.

Synthesis of the Stretchable, Self-Healing Ionic Hydrogel. The ionic hydrogel was fabricated through a one-pot and freezing/thawing method.[36] Briefly, 2.0 g of PVA, 1.0 g of PEI, and 4.0 g of LiCl were dissolved in 9 mL of deionized water to form a homogeneous solution in a 95 °C water bath with vigorous stirring for 1 h. Then, the uniform sol was shaped into a thin film in glass mold and then frozen at −20 °C overnight and thawed at room temperature for 12 h. The as-fabricated ionic hydrogel was cut into desired sizes for further measurement.

Fabrication of the Friction Layers. Silicone film and parylene-C deposited on VHB served as friction layers face to face. The silicone film was prepared by casting molding. The custom-made models with different microstructures were made of polylactic acid (PLA) by a 3D printer (Raize 3D N2 plus). Firstly, mix amounts of parts A and B of Ecoflex 00-30 in a ratio of 1:1 by weighing thoroughly. The well-mixed liquid was transferred to the model, and the surface was kept flat. The bubbles in the gel liquid were removed by a vacuum pumping. After cross-linking at 60 °C for 2 h, silicone film was obtained. The other friction layer was fabricated by evaporating and depositing parylene-C on VHB. Briefly, the parylene particles steamed at 120 °C and then deposited on one surface of VHB (the other surface was protected by mask), where the thickness of parylene and VHB are 0.3 μm and 1 mm. The conceptual diagram of the preparation process is shown in Figure S1.

Fabrication of TSAS. The TSAS was fabricated layer by layer in required sizes. The self-healing electrode was sealed by a bare VHB and a VHB loaded with parylene-C on one side, depending on the intrinsic viscosity of VHB. Then, silicone film was attached to the parylene layer with the help of VHB. The top surface of the packing layer was deposited with parylene-C. The TSAS was obtained with seven layers: displayed from top to bottom as parylene-C, VHB, silicone, parylene-C, VHB, self-healing electrode, VHB, respectively.

Characterization and Measurement of TSAS. Tensile test of the ionic hydrogel was performed by ESM301/Mark-10 system with a tensile speed of 50 mm·min^{-1}. The conductivity of the ionic hydrogel at different healing time was tested by Semiconductor Analysis System (Keithley 4200A-SCS). The optical images of the ionic hydrogel self-healing process were taken by a metallomicroscope (Nikon LV100ND). The scanning electron microscopy (SEM) images of silicone film were taken by a Hitachi field emission scanning electron microscope (SU 8020). The I_{sc} and Q_{sc} were detected by an electrometer (Keithley 6517B) and recorded by an oscilloscope (Teledyne LeCroy HDO6104). The V_{oc} was detected by an oscilloscope (Teledyne LeCroy HDO6104). A linear motor (LinMot E1100) was used to apply a periodic stable force on TSAS to perform a fatigue test. Vibration table (VT-500, YMC PIEZORONICS.INC) was employed as a high-frequency vibrator to test the response time (frequency, 500 Hz). In the investigation of the relationship between applied force and V_{oc} of TSAS, the ESM301/Mark-10 system was used to apply a periodic stable force on TSAS, and the corresponding voltage was recorded by oscilloscope. The force distribution simulation on TSAS was analyzed by a finite element simulation with COMSOL software. During muscle strength monitoring, the singles of V_{oc} produced by the movement of the biceps brachii, triceps brachii, and elbow were synchronously recorded by the oscilloscope (HDO8108A) with eight channels system.

ASSOCIATED CONTENT

Supporting Information

The Supporting Information is available free of charge at https://pubs.acs.org/doi/10.1021/acsnano.1c02010.

Movie S1: The self-healing of the electrode (MP4)
Movie S2: The detect limit of TSAS (MP4)
Movie S3: The self-healing ability of TSAS (MP4)
Movie S4: The relationship of V_{oc} and force (MP4)

https://doi.org/10.1021/acsnano.1c02010
ACS Nano XXXX, XXX, XXX−XXX

Movie S5: TSAS used in muscle function assessment (male) (MP4)

Movie S6: TSAS used in muscle function assessment (female) (MP4)

Movie S7: TSAS used in real-time muscle function assessment (MP4)

Preparation process and SEM images of friction layer; images of assembly layers and spherical crown's surface area; electrical output and fatigue performance of the TSAS; equation of the spherical crown's surface area; data and equation of the relationship of output and the deformation of TSAS; the relationship of applied force and output of TSAS; muscle function monitoring data of TSAS for other volunteers; wireless transmission module used in real-time muscle function assessment (PDF)

AUTHOR INFORMATION

Corresponding Authors

Yusheng Li − *Department of Orthopedics, Xiangya Hospital, Central South University, Changsha 410008, China*; Email: liyusheng@csu.edu.cn

Zhou Li − *CAS Center for Excellence in Nanoscience, Beijing Key Laboratory of Micro-nano Energy and Sensor, Beijing Institute of Nanoenergy and Nanosystems, Chinese Academy of Sciences, Beijing 101400, China; School of Nanoscience and Technology, University of Chinese Academy of Sciences, Beijing 100049, China*; orcid.org/0000-0002-9952-7296; Email: zli@binn.cas.cn

Authors

Chan Wang − *CAS Center for Excellence in Nanoscience, Beijing Key Laboratory of Micro-nano Energy and Sensor, Beijing Institute of Nanoenergy and Nanosystems, Chinese Academy of Sciences, Beijing 101400, China; School of Nanoscience and Technology, University of Chinese Academy of Sciences, Beijing 100049, China*; orcid.org/0000-0001-6002-5304

Xuecheng Qu − *CAS Center for Excellence in Nanoscience, Beijing Key Laboratory of Micro-nano Energy and Sensor, Beijing Institute of Nanoenergy and Nanosystems, Chinese Academy of Sciences, Beijing 101400, China; School of Nanoscience and Technology, University of Chinese Academy of Sciences, Beijing 100049, China*

Qiang Zheng − *CAS Center for Excellence in Nanoscience, Beijing Key Laboratory of Micro-nano Energy and Sensor, Beijing Institute of Nanoenergy and Nanosystems, Chinese Academy of Sciences, Beijing 101400, China; School of Nanoscience and Technology, University of Chinese Academy of Sciences, Beijing 100049, China*

Ying Liu − *CAS Center for Excellence in Nanoscience, Beijing Key Laboratory of Micro-nano Energy and Sensor, Beijing Institute of Nanoenergy and Nanosystems, Chinese Academy of Sciences, Beijing 101400, China; School of Nanoscience and Technology, University of Chinese Academy of Sciences, Beijing 100049, China*

Puchuan Tan − *CAS Center for Excellence in Nanoscience, Beijing Key Laboratory of Micro-nano Energy and Sensor, Beijing Institute of Nanoenergy and Nanosystems, Chinese Academy of Sciences, Beijing 101400, China; Beijing Advanced Innovation Centre for Biomedical Engineering, Key Laboratory for Biomechanics and Mechanobiology of Ministry of Education, School of Biological Science and Medical Engineering, Beihang University, Beijing 100191, China*

Bojing Shi − *CAS Center for Excellence in Nanoscience, Beijing Key Laboratory of Micro-nano Energy and Sensor, Beijing Institute of Nanoenergy and Nanosystems, Chinese Academy of Sciences, Beijing 101400, China; Beijing Advanced Innovation Centre for Biomedical Engineering, Key Laboratory for Biomechanics and Mechanobiology of Ministry of Education, School of Biological Science and Medical Engineering, Beihang University, Beijing 100191, China*

Han Ouyang − *CAS Center for Excellence in Nanoscience, Beijing Key Laboratory of Micro-nano Energy and Sensor, Beijing Institute of Nanoenergy and Nanosystems, Chinese Academy of Sciences, Beijing 101400, China; Beijing Advanced Innovation Centre for Biomedical Engineering, Key Laboratory for Biomechanics and Mechanobiology of Ministry of Education, School of Biological Science and Medical Engineering, Beihang University, Beijing 100191, China*

Shengyu Chao − *CAS Center for Excellence in Nanoscience, Beijing Key Laboratory of Micro-nano Energy and Sensor, Beijing Institute of Nanoenergy and Nanosystems, Chinese Academy of Sciences, Beijing 101400, China; School of Nanoscience and Technology, University of Chinese Academy of Sciences, Beijing 100049, China*

Yang Zou − *CAS Center for Excellence in Nanoscience, Beijing Key Laboratory of Micro-nano Energy and Sensor, Beijing Institute of Nanoenergy and Nanosystems, Chinese Academy of Sciences, Beijing 101400, China; School of Nanoscience and Technology, University of Chinese Academy of Sciences, Beijing 100049, China*

Chaochao Zhao − *CAS Center for Excellence in Nanoscience, Beijing Key Laboratory of Micro-nano Energy and Sensor, Beijing Institute of Nanoenergy and Nanosystems, Chinese Academy of Sciences, Beijing 101400, China; Department of Biomedical Engineering, School of Medical Engineering, Foshan University, Foshan 528225, China*

Zhuo Liu − *CAS Center for Excellence in Nanoscience, Beijing Key Laboratory of Micro-nano Energy and Sensor, Beijing Institute of Nanoenergy and Nanosystems, Chinese Academy of Sciences, Beijing 101400, China; Beijing Advanced Innovation Centre for Biomedical Engineering, Key Laboratory for Biomechanics and Mechanobiology of Ministry of Education, School of Biological Science and Medical Engineering, Beihang University, Beijing 100191, China*

Complete contact information is available at: https://pubs.acs.org/10.1021/acsnano.1c02010

Author Contributions

The manuscript was written through the contributions of all authors. All authors have given approval to the final version of the manuscript. C.W., X.Q., and Q.Z. designed, fabricated, and tested the TSAS. C.W. and Y.Liu synthesized and characterized the ionic gel. C.W., X.Q., and S.C. performed the experiment about the relationship of the output of TSAS and applied force as well as analyzed data. C.W., X.Q., Q.Z., Y.Liu, and P.T. performed the muscle function monitoring study. C.W., X.Q., and Q.Z. wrote the manuscript. H.O., B.S., Y.Z., and Z.Liu made the contribution in the theoretical explanation and the article revises. Z.Li and Y.Li. designed and guided the project.

https://doi.org/10.1021/acsnano.1c02010
ACS Nano XXXX, XXX, XXX−XXX

Author Contributions

#C.W., X.Q., and Q.Z. contributed equally to this work.

Notes

The authors declare no competing financial interest.

ACKNOWLEDGMENTS

This work was supported by the Key-Area Research and Development Program of Guangdong Province (2018B030331001), National Natural Science Foundation of China (61875015, 81874030, 82001982), the Beijing Natural Science Foundation (JQ20038, 7204275, 7204333), Fundamental Research Funds for the Central Universities, and the National Youth Talent Support Program.

REFERENCES

(1) Aoyagi, Y.; Shephard, R. J. Aging and Muscle Function. *Sports Med.* **1992**, *14*, 376−396.
(2) Pfeifer, M.; Begerow, B.; Minne, H. W. Vitamin D and Muscle Function. *Osteoporosis Int.* **2002**, *13*, 187−94.
(3) Symonds, T.; Campbell, P.; Randall, J. A. A Review of Muscle and Performance-Based Assessment Instruments in DM1. *Muscle Nerve* **2017**, *56*, 78−85.
(4) Ibitoye, M. O.; Hamzaid, N. A.; Zuniga, J. M.; Abdul, W. A. K. Mechanomyography and Muscle Function Assessment: A Review of Current State and Prospects. *Clin. Biomech. (Bristol, Avon)* **2014**, *29*, 691−704.
(5) Toigo, M.; Fluck, M.; Riener, R.; Klamroth-Marganska, V. Robot-Assisted Assessment of Muscle Strength. *J. Neuroeng. Rehabil.* **2017**, *14*, 103.
(6) Jones, Ma; Stratton, G. Muscle Function Assessment in Children. *Acta Paediatr.* **2000**, *89*, 753−761.
(7) Cuthbert, S. C.; Goodheart, G. J., Jr. On the Reliability and Validity of Manual Muscle Testing: A Literature Review. *Chiropr. Osteopat.* **2007**, *15*, 4.
(8) Bohannon, R. W. Hand-Grip Dynamometry Predicts Future Outcomes in Aging Adults. *J. Geriat. Phys. Ther.* **2008**, *31*, 3−10.
(9) Wang, G.; Feng, H.; Hu, L.; Jin, W.; Hao, Q.; Gao, A.; Peng, X.; Li, W.; Wong, K. Y.; Wang, H.; Li, Z.; Chu, P. K. An Antibacterial Platform Based on Capacitive Carbon-Doped TiO2 Nanotubes after Direct or Alternating Current Charging. *Nat. Commun.* **2018**, *9*, 2055.
(10) Fan, F.-R.; Tian, Z.-Q.; Wang, Z. L. Flexible Triboelectric Generator. *Nano Energy* **2012**, *1*, 328−334.
(11) Jeong, C. K.; Lee, J.; Han, S.; Ryu, J.; Hwang, G.-T.; Park, D. Y.; Park, J. H.; Lee, S. S.; Byun, M.; Ko, S. H.; Lee, K. J. A Hyper-Stretchable Elastic-Composite Energy Harvester. *Adv. Mater.* **2015**, *27*, 2866−2875.
(12) Parida, K.; Kumar, V.; Wang, J.; Bhavanasi, V.; Bendi, R.; Lee, P. S. Highly Transparent, Stretchable, and Self-Healing Ionic-Skin Triboelectric Nanogenerators for Energy Harvesting and Touch Applications. *Adv. Mater.* **2017**, *29*, 1702181.
(13) Shi, M.; Zhang, J.; Chen, H.; Han, M.; Shankaregowda, S. A.; Su, Z.; Meng, B.; Cheng, X.; Zhang, H. Self-Powered Analogue Smart Skin. *ACS Nano* **2016**, *10*, 4083−4091.
(14) Chen, C.; Wen, Z.; Shi, J.; Jian, X.; Li, P.; Yeow, J. T. W.; Sun, X. Micro Triboelectric Ultrasonic Device for Acoustic Energy Transfer and Signal Communication. *Nat. Commun.* **2020**, *11*, 4143.
(15) Chandrasekhar, A.; Vivekananthan, V.; Kim, S.-J. A Fully Packed Spheroidal Hybrid Generator for Water Wave Energy Harvesting and Self-Powered Position Tracking. *Nano Energy* **2020**, *69*, 104439.
(16) Chandrasekhar, A.; Vivekananthan, V.; Khandelwal, G.; Kim, S. J. A Fully Packed Water-Proof, Humidity Resistant Triboelectric Nanogenerator for Transmitting Morse Code. *Nano Energy* **2019**, *60*, 850−856.
(17) Anaya, D. V.; Yuce, M. R. Stretchable Triboelectric Sensor for Measurement of the Forearm Muscles Movements and Fingers Motion for Parkinson's Disease Assessment and Assisting Technologies. *Med. Devices Sens.* **2021**, *4*, e10154.
(18) Guan, Q.; Lin, G.; Gong, Y.; Wang, J.; Tan, W.; Bao, D.; Liu, Y.; You, Z.; Sun, X.; Wen, Z.; Pan, Y. Highly Efficient Self-Healable and Dual Responsive Hydrogel-Based Deformable Triboelectric Nanogenerators for Wearable Electronics. *J. Mater. Chem. A* **2019**, *7*, 13948−13955.
(19) Wang, S.; Wang, X.; Wang, Z. L.; Yang, Y. Efficient Scavenging of Solar and Wind Energies in a Smart City. *ACS Nano* **2016**, *10*, 5696−700.
(20) Anaya, D. V.; He, T.; Lee, C.; Yuce, M. R. Self-Powered Eye Motion Sensor Based on Triboelectric Interaction and Near-Field Electrostatic Induction for Wearable Assistive Technologies. *Nano Energy* **2020**, *72*, 104675.
(21) Zou, Y.; Tan, P.; Shi, B.; Ouyang, H.; Jiang, D.; Liu, Z.; Li, H.; Yu, M.; Wang, C.; Qu, X.; Zhao, L.; Fan, Y.; Wang, Z. L.; Li, Z. A Bionic Stretchable Nanogenerator for Underwater Sensing and Energy Harvesting. *Nat. Commun.* **2019**, *10*, 2695.
(22) Shi, Q.; Wang, H.; Wang, T.; Lee, C. Self-Powered Liquid Triboelectric Microfluidic Sensor for Pressure Sensing and Finger Motion Monitoring Applications. *Nano Energy* **2016**, *30*, 450−459.
(23) Nayak, S.; Li, Y.; Tay, W.; Zamburg, E.; Singh, D.; Lee, C.; Koh, S. J. A.; Chia, P.; Thean, A. V.-Y. Liquid-Metal-Elastomer Foam for Moldable Multi-Functional Triboelectric Energy Harvesting and Force Sensing. *Nano Energy* **2019**, *64*, 103912.
(24) Wang, C.; Li, X.; Hu, H.; Zhang, L.; Huang, Z.; Lin, M.; Zhang, Z.; Yin, Z.; Huang, B.; Gong, H.; Bhaskaran, S.; Gu, Y.; Makihata, M.; Guo, Y.; Lei, Y.; Chen, Y.; Wang, C.; Li, Y.; Zhang, T.; Chen, Z.; et al. Monitoring of the Central Blood Pressure Waveform via a Conformal Ultrasonic Device. *Nat. Biomed. Eng.* **2018**, *2*, 687−695.
(25) Shin, J.; Yan, Y.; Bai, W.; Xue, Y.; Gamble, P.; Tian, L.; Kandela, I.; Haney, C. R.; Spees, W.; Lee, Y.; Choi, M.; Ko, J.; Ryu, H.; Chang, J.-K.; Pezhouh, M.; Kang, S.-K.; Won, S. M.; Yu, K. J.; Zhao, J.; Lee, Y. K.; et al. Bioresorbable Pressure Sensors Protected with Thermally Grown Silicon Dioxide for the Monitoring of Chronic Diseases and Healing Processes. *Nat. Biomed. Eng.* **2019**, *3*, 37−46.
(26) Sheng, H.; Wang, X.; Kong, N.; Xi, W.; Yang, H.; Wu, X.; Wu, K.; Li, C.; Hu, J.; Tang, J.; Zhou, J.; Duan, S.; Wang, H.; Suo, Z. Neural Interfaces by Hydrogels. *Extreme Mech. Lett.* **2019**, *30*, 100510.
(27) Wang, Y.; Zhu, C.; Pafattner, R.; Yan, H.; Jin, L.; Chen, S.; Molina-Lopez, F.; Lissel, F.; Liu, J.; Rabiah, N. I.; Chen, Z.; Chung, J. W.; Linder, C.; Toney, M. F.; Murmann, B. M.; Bao, Z. A Highly Stretchable, Transparent, and Conductive Polymer. *Sci. Adv.* **2017**, *3*, e1602076.
(28) Xu, S.; Jayaraman, A.; Rogers, J. A. Skin Sensors Are the Future of Health Care. *Nature* **2019**, *571*, 319−321.
(29) Choi, S.; Han, S. I.; Jung, D.; Hwang, H. J.; Lim, C.; Bae, S.; Park, O. K.; Tschabrunn, C. M.; Lee, M.; Bae, S. Y.; Yu, J. W.; Ryu, J. H.; Lee, S. W.; Park, K.; Kang, P. M.; Lee, W. B.; Nezafat, R.; Hyeon, T.; Kim, D. H. Highly Conductive, Stretchable and Biocompatible Ag-Au Core-Sheath Nanowire Composite for Wearable and Implantable Bioelectronics. *Nat. Nanotechnol.* **2018**, *13*, 1048−1056.
(30) Parida, K.; Thangavel, G.; Cai, G.; Zhou, X.; Park, S.; Xiong, J.; Lee, P. S. Extremely Stretchable and Self-Healing Conductor Based on Thermoplastic Elastomer for All-Three-Dimensional Printed Triboelectric Nanogenerator. *Nat. Commun.* **2019**, *10*, 2158.
(31) Sun, J.; Pu, X.; Liu, M.; Yu, A.; Du, C.; Zhai, J.; Hu, W.; Wang, Z. L. Self-Healable, Stretchable, Transparent Triboelectric Nanogenerators as Soft Power Sources. *ACS Nano* **2018**, *12*, 6147−6155.
(32) Chen, Y.; Pu, X.; Liu, M.; Kuang, S.; Zhang, P.; Hua, Q.; Cong, Z.; Guo, W.; Hu, W.; Wang, Z. L. Shape-Adaptive, Self-Healable Triboelectric Nanogenerator with Enhanced Performances by Soft Solid-Solid Contact Electrification. *ACS Nano* **2019**, *13*, 8936.
(33) Lee, J. H.; Hinchet, R.; Kim, S. K.; Kim, S.; Kim, S.-W. Shape Memory Polymer-Based Self-Healing Triboelectric Nanogenerator. *Energy Environ. Sci.* **2015**, *8*, 3605−3613.
(34) Lai, Y. C.; Wu, H. M.; Lin, H. C.; Chang, C. L.; Chou, H. H.; Hsiao, Y. C.; Wu, Y. C. Entirely, Intrinsically, and Autonomously Self-Healable, Highly Transparent, and Superstretchable Triboelectric

Nanogenerator for Personal Power Sources and Self-Powered Electronic Skins. *Adv. Funct. Mater.* **2019**, *29*, 1904626.
(35) Son, D.; Kang, J.; Vardoulis, O.; Kim, Y.; Matsuhisa, N.; Oh, J. Y.; To, J. W. F.; Mun, J.; Katsumata, T.; Liu, Y.; McGuire, A. F.; Krason, M.; Molina-Lopez, F.; Ham, J.; Kraft, U.; Lee, Y.; Yun, Y.; Tok, B.-H. J.; Bao, Z. An Integrated Self-Healable Electronic Skin System Fabricated via Dynamic Reconstruction of a Nanostructured Conducting Network. *Nat. Nanotechnol.* **2018**, *13*, 1057−1065.
(36) Chen, Y.; Qian, W.; Chen, R.; Zhang, H.; Li, X.; Shi, D.; Dong, W.; Chen, M.; Zhao, Y. One-Pot Preparation of Autonomously Self-Healable Elastomeric Hydrogel from Boric Acid and Random Copolymer Bearing Hydroxyl Groups. *ACS Macro Lett.* **2017**, *6*, 1129−1133.
(37) Li, H.; Wang, X.; Jiang, W.; Fu, H.; Liang, X.; Zhang, K.; Li, Z.; Zhao, C.; Feng, H.; Nie, J.; Liu, R.; Zhou, G.; Fan, Y.; Li, Z. Alkali Metal Chlorides Based Hydrogel as Eco-Friendly Neutral Electrolyte for Bendable Solid-State Capacitor. *Adv. Mater. Interfaces* **2018**, *5*, 1701648.
(38) Filippidi, E.; Cristiani, T. R.; Eisenbach, C. D.; Waite, J. H.; Israelachvili, J. N.; Ahn, B. K.; Valentine, M. T. Toughening Elastomers Using Musselinspired Iron-Catechol Complexes. *Science* **2017**, *358*, 502−505.
(39) Yang, H.; Li, C.; Tang, J.; Suo, Z. Strong and Degradable Adhesion of Hydrogels. *ACS Appl. Bio. Mater.* **2019**, *2*, 1781−1786.
(40) Jeon, I.; Cui, J.; Illeperuma, W. R.; Aizenberg, J.; Vlassak, J. J. Extremely Stretchable and Fast Self-Healing Hydrogels. *Adv. Mater.* **2016**, *28*, 4678−83.
(41) Boutry, C. M.; Kaizawa, Y.; Schroeder, B. C.; Chortos, A.; Legrand, A.; Wang, Z.; Chang, J.; Fox, P.; Bao, Z. A Stretchable and Biodegradable Strain and Pressure Sensor for Orthopaedic Application. *Nat. Electron.* **2018**, *1*, 314−321.
(42) Ouyang, H.; Liu, Z.; Li, N.; Shi, B.; Zou, Y.; Xie, F.; Ma, Y.; Li, Z.; Li, H.; Zheng, Q.; Qu, X.; Fan, Y.; Wang, Z. L.; Zhang, H.; Li, Z. Symbiotic Cardiac Pacemaker. *Nat. Commun.* **2019**, *10*, 1821.
(43) Liu, Z.; Ma, Y.; Ouyang, H.; Shi, B.; Li, N.; Jiang, D.; Xie, F.; Qu, D.; Zou, Y.; Huang, Y.; Li, H.; Zhao, C.; Tan, P.; Yu, M.; Fan, Y.; Zhang, H.; Wang, Z. L.; Li, Z. Transcatheter Self-Powered Ultrasensitive Endocardial Pressure Sensor. *Adv. Funct. Mater.* **2019**, *29*, 1807560.
(44) Chen, Y.; Wang, Y.-C.; Zhang, Y.; Zou, H.; Lin, Z.; Zhang, G.; Zou, C.; Wang, Z. L. Elastic-Beam Triboelectric Nanogenerator for High-Performance Multifunctional Applications: Sensitive Scale, Acceleration/Force/Vibration Sensor, and Intelligent Keyboard. *Adv. Energy Mater.* **2018**, *8*, 1802159.
(45) Wang, Z. L. On Maxwell's Displacement Current for Energy and Sensors: The Origin of Nanogenerators. *Mater. Today* **2017**, *20*, 74−82.
(46) Khan, U.; Kim, T. H.; Ryu, H.; Seung, W.; Kim, S. W. Graphene Tribotronics for Electronic Skin and Touch Screen Applications. *Adv. Mater.* **2017**, *29*, 1603544.
(47) Chandrasekhar, A.; Vivekananthan, V.; Khandelwal, G.; Kim, S.-J. Sustainable Human-Machine Interactive Triboelectric Nanogenerator toward a Smart Computer Mouse. *ACS Sustainable Chem. Eng.* **2019**, *7*, 7177−7182.
(48) Chandrasekhar, A.; Khandelwal, G.; Alluri, N. R.; Vivekananthan, V.; Kim, S.-J. Battery-Free Electronic Smart Toys: A Step toward the Commercialization of Sustainable Triboelectric Nanogenerators. *ACS Sustainable Chem. Eng.* **2018**, *6*, 6110−6116.

https://doi.org/10.1021/acsnano.1c02010
ACS Nano XXXX, XXX, XXX−XXX